Geophysical Research Letters

RESEARCH LETTER
10.1029/2020GL088681

Numerical Simulation-Based Clarification of a Fluid-Flow System in a Seafloor Hydrothermal Vent Area in the Middle Okinawa Trough

S. A. Tomita[1], K. Koike[1], T. Goto[1,2], and K. Suzuki[3]

[1]Department of Urban Management, Graduate School of Engineering, Kyoto University, Kyoto, Japan, [2]Now at Graduate School of Life Science, University of Hyogo, Hyogo, Japan, [3]Submarine Resources Research Center, Japan Agency for Marine-Earth Science and Technology (JAMSTEC), Kanagawa, Japan

Key Points:
- Numerical simulation of multiphase fluid flow revealed regional temperature, fluid-flow patterns, and physical property distributions
- Integration of results with geologic interpretations provided a plausible generation mechanism of seafloor massive sulfide deposits
- Formation of caprocks below the seafloor induces boiling and lateral flow of hydrothermal fluid and, consequently, the deposit generation

Supporting Information:
- Supporting Information S1

Correspondence to:
S. A. Tomita,
tomita.shohei.57n@st.kyoto-u.ac.jp

Citation:
Tomita, S. A., Koike, K., Goto, T., & Suzuki, K. (2020). Numerical simulation-based clarification of a fluid-flow system in a seafloor hydrothermal vent area in the middle Okinawa Trough. *Geophysical Research Letters*, *47*, e2020GL088681. https://doi.org/10.1029/2020GL088681

Received 6 MAY 2020
Accepted 6 OCT 2020
Accepted article online 13 OCT 2020

Abstract Despite many studies on seafloor hydrothermal systems conducted to date, the generation mechanism of seafloor massive sulfide (SMS) deposits is not yet fully understood. To elucidate this mechanism, this study clarifies the three-dimensional regional temperature distribution and fluid flow of a seafloor hydrothermal system of the Iheya North Knoll, middle Okinawa Trough. Lateral flow and boiling of hydrothermal fluids below a caprock were the main features found by the simulation. A caprock formation generated by anhydrite precipitation and hydrothermal alteration is the most plausible cause of these features, because caprocks can increase the temperature and induce boiling of fluids by preventing seawater inflow. Such a formation also gradually makes the top of the conduit less permeable; thus, lateral flow occurs. Consequently, vapor-rich hydrothermal fluids poor in metals are discharged from vents as white smokers, whereas liquid-dominated hydrothermal fluids rich in metals flow laterally below the caprocks, forming subseafloor SMS deposits.

Plain Language Summary In seafloor hydrothermal systems, the seawater heated by magma circulates under the seafloor and forms seafloor massive sulfide (SMS) deposits. Recently, SMS deposits have attracted interest as a new metal resource, the generation mechanism and model of which must be established for accurate resource exploration. However, the mechanism is not yet fully understood. To address this problem, we applied a hydrothermal flow simulation and clarified the temperature distribution and fluid flow in the Iheya North Knoll, southwestern Japan. The result revealed that lateral flow and boiling of hydrothermal fluids occur below the seafloor. A low permeability caprock formation generated by anhydrite and clay mineral development is the most plausible cause of these occurrences, because a caprock can increase the temperature and induce boiling of fluids by suppressing the seawater inflow. This formation also makes fluid outlets less permeable, thus induces lateral flow. Consequently, vapor-rich hydrothermal fluids poor in metals are discharged from vents, while liquid-dominated hydrothermal fluids rich in metals flow laterally below the caprocks, forming subseafloor SMS deposits.

1. Introduction

Recent rapid expansion of the world economy, population growth, rising demand for and prices of metals, and uneven distribution of resources induce global risks against the stable supply of metal resources (Bardi et al., 2016; Lusty & Gunn, 2015). For the supply, in the exploration of metal deposits, deeper and deeper parts of the crust are being explored, and efforts are extending to the seafloor from the land. In these zones, finding new deposits becomes more and more difficult because of decreases in the amount and spatial resolution of survey data.

Because hydrothermal circulation below the seafloor promotes chemical reaction, heat transfer, and mutual interaction between the crust and ocean (Alt, 1995; Stein & Stein, 1992; Tivey, 2007), more than 300 high-temperature vent sites, which are potential fields of metal deposits, have been found to date in mid-ocean ridges (65%), along volcanic arcs (12%), and at back-arc spreading centers (22%) (Hannington et al., 2011). Seafloor massive sulfide (SMS) deposits are the most typical type formed in such hydrothermal systems accompanying high contents of base metals (copper, zinc, and lead) and precious metals (silver and gold) (Spagnoli et al., 2016). SMS deposits are regarded as important near-future mining targets because of their considerable reserves and high metal grades (Lipton, 2012). For efficient mining and development,

understanding the locations, configurations, grade distributions, and genesis of such deposits is of the utmost importance.

Of particular interest in SMS deposits is the presence of two types: one formed in seafloor mounds and black smoker chimneys under oxic environments and another formed below the seafloor by mineral replacement (Tornos et al., 2015). Coexistence of these types was estimated recently from a two-layered low resistivity zones (of 0.2 Ohm-m or less) by a marine electrical resistivity tomography in the Iheya North Knoll in the middle Okinawa Trough, southwest of Japan (Ishizu et al., 2019). The structure was interpreted as two mineralization zones on the seafloor and at about 40 m below seafloor (mbsf). In addition, similar two or multilayered SMS deposits were also found by drillings in the Okinawa Trough (Saito et al., 2015; Yoshizumi et al., 2015). To date, various SMS mineralization models have been developed (Tornos et al., 2015). However, most are based on qualitative, geological observations, and the concrete physical setting that caused generation of the deposits (temperature, pressure, heat flux, and fluid flow) has not yet been elucidated; for example, the above-mentioned two-layered mineralization structure has not been explained by any quantitative models. The physical setting can be elucidated only through numerical simulation, because it is not possible to accurately observe the setting and the phenomena that occur there under progress over a long time and a wide area below the seafloor.

Based on that background, this study aims to build a three-dimensional (3-D) numerical model that can correctly represent a seafloor hydrothermal system in a back-arc basin with geological, hydrological, and thermal constraints, clarify the above physical setting, and present a generation mechanism of the two-layered SMS structure by selecting the Iheya North Knoll as a case area (Figure 1a). Two or more mineralization styles are commonly mixed in SMS deposits (Tornos et al., 2015). Therefore, this study, perhaps the first study conducted for the above purposes, can contribute to understanding the generation setting of complex (two-layered or multilayered) SMS deposits in other areas.

2. Data and Methods

The study area is situated in a back-arc basin between the Ryukyu arc-trench system and the Eurasian continent (Figure 1a); the main hydrothermal area is 500 m × 300 m in size (Figure 1b). Nine sites of representative active hydrothermal vents have been discovered in this area (Kawagucci et al., 2011); among them, the North Big Chimney (NBC) is known to have the highest temperature (311°C) and the largest flow rate recorded thus far (Takai & Nakamura, 2010), suggesting that the NBC is located on the main flow path.

The Iheya North Knoll is composed of (i) volcanic rocks forming knolls and (ii) thick sediments over the rocks in the central depression; volcaniclastic pumiceous deposits with widely distributed hard layers, perhaps impermeable caprocks, are estimated to be the main sedimentary components based on seismic survey results (Tsuji et al., 2012). Detailed lithology was revealed by drilling surveys at five sites in a program of the Integrated Ocean Drilling Program (IODP) Expedition 331 (Figure 1b) (Takai et al., 2011): The sediments are alternating sequences of hard low-porosity and porous pumiceous layers, mainly composed of pelagic and hemipelagic mud and volcaniclastic pumiceous deposits with hydrothermal alteration. Abundant anhydrite greatly reduces the porosity by filling voids in sediments and consequently forms the low-porosity layers. Anhydrite precipitates from hydrothermal fluid when mixed with seawater (Lowell et al., 2003; Lowell & Yao, 2002). Low-porosity layers rich in anhydrite are regarded to act as impermeable caprocks that blocks vertical fluid flows.

Because backarcs exist under extensional tectonic settings, normal faults, tensile fractures, and fracture zones develop parallel to the extension axis and act as fluid conduits (Sahlström et al., 2018). Following this general rule, several N-S faults are developed in the study area, on which the main hydrothermal mounds are located (Figure 1b). Research on modern (Arai et al., 2018; Tivey & Johnson, 2002) and fossil hydrothermal systems (Coogan et al., 2006) has drawn an image wherein hydrothermal upflows are concentrated in tube-like conduits, which presumably continue to the reaction zone (Tivey & Johnson, 2002). In fact, several tube-like conduits under mounds were detected from the seismic survey results in the Okinawa Trough (Arai et al., 2018; Tsuji et al., 2012), including a tube-like seismically transparent structure, which probably represents a conduit, under the NBC mound (Takai et al., 2010).

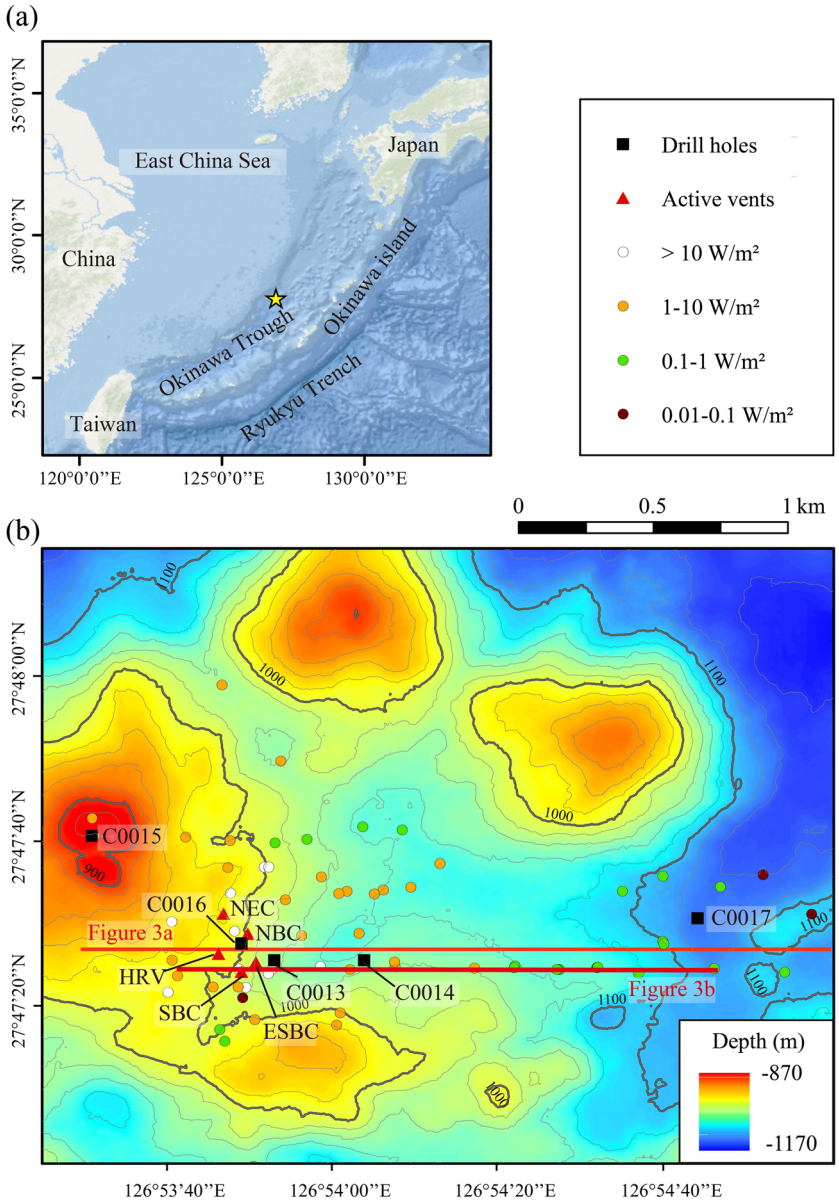

Figure 1. (a) Location of the Iheya north hydrothermal field in the middle Okinawa trough marked by a star symbol and (b) bathymetry map of the study area with IODP drilling sites (black squares), active vent sites (red triangles), and heat flux measurement points (circles as in the legend, after Masaki et al., 2011). Two red lines show the locations of Figures 3a and 3b.

Using the above-mentioned accessible geological and geophysical data, a numerical model of the study area, 1.2 km (N-S) × 4.0 km (E-W) × 1.6 km (vertical below the seafloor) in size, was constructed (Figure 2) to simulate hydrothermal fluid flow of pure water based on Darcy's law and the mass and energy conservation equations. The TOUGH2 software was used for the simulation because of its high capability of analyzing gas-liquid two-phase flow and 3-D heat flow (Pruess et al., 1999). A buffer zone 10 km in size was set around the model domain (Figures 2a and 2c), and the domain was discretized by Voronoi cells with 0.5 to 500 m thickness from the shallow to deep parts and 30 to 2,000 m side length from the middle conduit to domain peripheral zones (Figure 2a). The bathymetric data of the top of the domain were acquired by a multibeam echosounder system (MBES) during several cruises. We set the initial conditions as hydrostatic pressure and 4°C at the seafloor with the average thermal gradient in the study area, 0.12°C/m, except for the vent sites thermal gradient (Masaki et al., 2011); the surface boundary condition was set as a permeable boundary

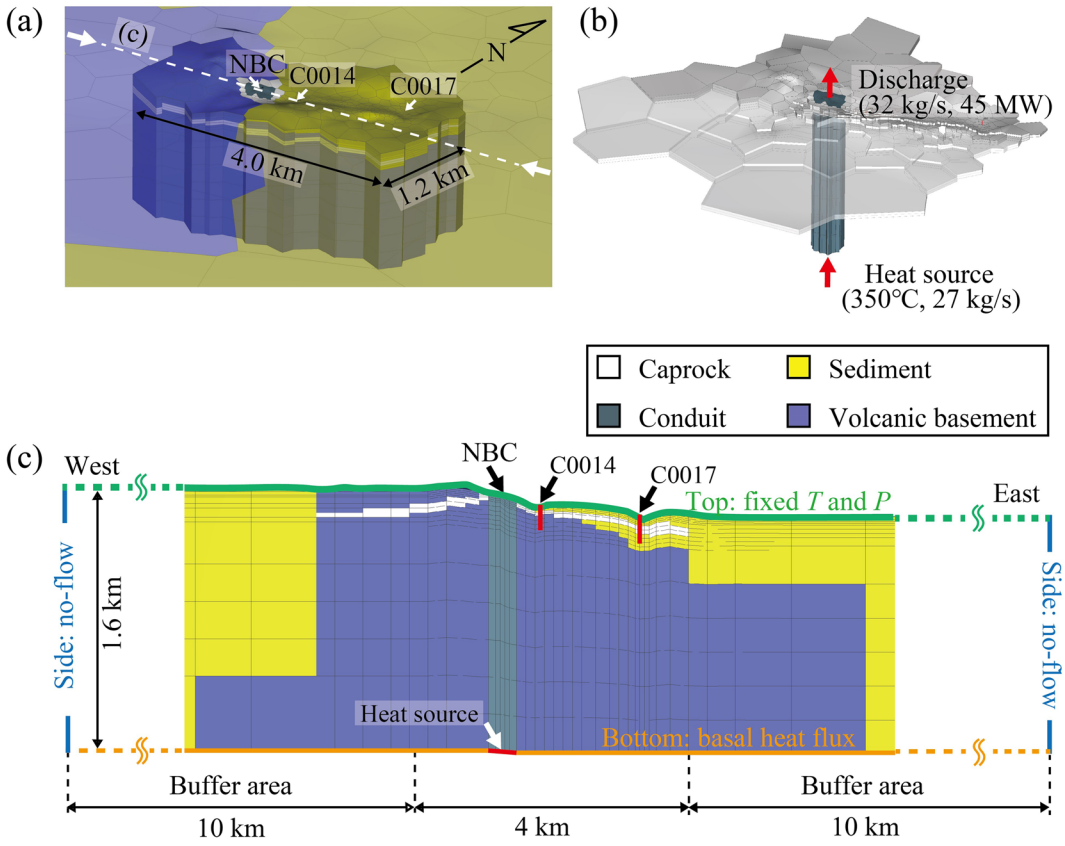

Figure 2. Calculation model. (a) Perspective view of the model domain with a buffer zone of 10 km, shown as semitransparent, set around the domain. Voronoi cell sizes become smaller toward the domain center. The broken white line shows the location of Figure 2c. (b) Distributions of a caprock layer and a vertical conduit zone. (c) Detailed configuration of cells and geologic structure composed of four elements along an E-W cross-section in Figure 2a with the model size and boundary conditions. The cell thickness was set as 0.5 m (thinnest) near the seafloor (the top boundary), because the heat fluxes were measured at the top subsurface below the seafloor (Masaki et al., 2011), and the thickness gradually increases with depth, with 0.5 m for top five layers, 10 m for the next five layers, 25 m for six layers, and 200 m for the bottom seven layers.

of the seafloor with constant temperature, 4°C, and hydrostatic pressure, and the side and bottom boundaries were set as impermeable.

To clarify the general fluid flow pattern and temperature and pressure distributions, the model domain was simply divided into four geologic elements, conduit, caprock, sediment, and volcanic basement, by excluding geological and hydrological heterogeneities. These elements were assigned in the model domain based on the drilling and seismic survey data. A highly permeable conduit 300 m in diameter was set vertically from the seafloor to the bottom of the model domain as the main discharge area, by locating the NBC as the center of conduit (Figure 2b). Distributions of the volcanic basement, sediment, and a continuous caprock layer 5 to 100 m in thickness were set following the report of Takai et al. (2011) (Figure 2c). In addition, for the physical rock properties, the density, porosity, and thermal conductivity of the four elements were set based on drilling survey data, and permeability was set based on the literature data described in the supporting information Text S1 (see also Table S1).

The validity of the constructed calculation model was checked by comparing the calculated temperature and heat flux with those obtained by measurement. A wide range of heat flux (0.01–100 W/m^2) was observed at 78 points with exceedingly high values around the NBC mound (Masaki et al., 2011). A noteworthy trend was that heat flux decreased with increasing distance from the mound (Figure 1b) to very low heat flux (<0.1 W/m^2) 2 km from the mound, suggesting an occurrence of several-km-scale fluid circulation. In addition, temperature logging data were obtained at Sites C0014 and C0017 (Figure 3d) (Takai et al., 2011).

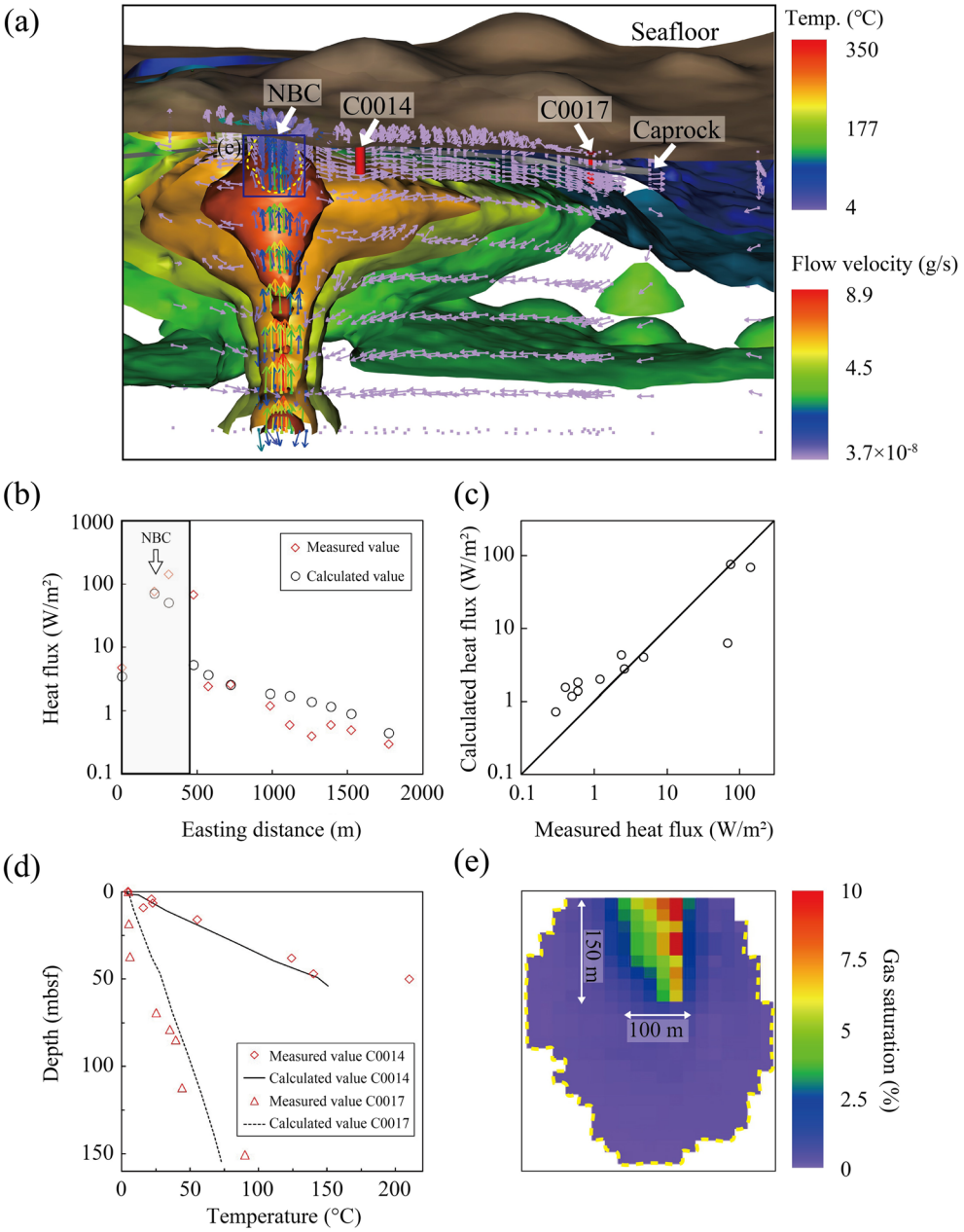

Figure 3. Simulation results and verification. (a) 3-D view of iso-temperature surfaces and fluid flow vectors (arrows) on an E-W cross-section along the profile shown in Figure 1b. Boiling zone around the NBC is delineated by the broken yellow line. The thick red lines, brown surface, and gray surface in the shallow subseafloor denote the seafloor drillings with site names, the seafloor, and the caprock layer, respectively. (b) Comparison of calculated heat fluxes with the measurement data after Masaki et al. (2011). The easting distance is along the profile shown in Figure 1b. The gray hatched part from 0 to 450 m distance denotes the active hydrothermal area. (c) Cross-plot of calculated heat flux and measured ones. (d) Comparison of calculated temperatures with the measurement data at sites C0014 and C0017 after Takai et al. (2011). (e) Vertical cross-section of gas saturation distribution in the boiling zone shown in Figure 3a.

Temperature data obtained at the distal flank at Site C0017 showed 44°C at 112 mbsf and 90°C at 151 mbsf, which imply cold seawater recharge into the hydrothermal system. In contrast, the temperature at Site C0014 at the intermediate flank was 22°C at 6.5 mbsf, and a high thermal gradient was observed below 10 mbsf with temperatures of 55°C at 16 mbsf, 150°C at 47 mbsf, and 210°C at only 50 mbsf. The temperature profiles at Sites C0014 and C0017 did not show simple increases with depth, suggesting the occurrence of lateral flow.

The injection rate and discharge rate at the conduit from the bottom and top boundaries, respectively, and the permeabilities of the four elements were adjusted with trial-and-error approaches so that the heat flux and temperature differences would be acceptably small with consideration of heat balance, as explained in Text S2. The resultant injection rate and discharge rate with the best matches were 27 kg/s ($=4 \times 10^{-4}$ kg/(s·m^2)) of 350°C fluid and 32 kg/s (=45 MW heat flow), respectively. Under those conditions, the steady state was simulated.

3. Results and Discussion

The steady state flows are mostly upflows along the conduit and discharge from the seafloor, and partly lateral flows along the caprock form a mushroom-shaped high-temperature region (Figure 3a; see also Figure S1 in a cross-section view). Another main flow is descending low-temperature seawater from the seafloor near the volcanic ridge, about 2 km away from the NBC mound at the eastern Site C0017, toward the conduit, which subsequently induces flow circulation. The occurrences of lateral flow below the caprock and downward seawater flow in that place agree with interpretations based on the chemical compositions of the pore waters (Ishibashi et al., 2017) and heat flux and seismic survey data (Masaki et al., 2011; Tsuji et al., 2012).

The correctness of the simulation results can be confirmed by the findings that the calculated heat fluxes almost agree with the measured ones (Figure 3b) and that the calculated temperatures generally agree with the measured ones except for the underestimation for the deepest, 50 mbsf data of Site C0014 (Figure 3d). The consistency of heat flux can be more clearly confirmed by a cross-plot of the calculated and measured heat flux values (Figure 3c). The differences between the calculation and measurement results are attributed to the simplified geologic model that did not incorporate local changes in hydraulic parameters.

A noteworthy feature revealed by the simulation is an occurrence of boiling in the depth range between the surface of the NBC and 150 mbsf in the conduit, caused by a pressure drop at the top of the ascending hydrothermal fluids (Figure 3e). The gas saturation rate reaches a maximum (10%) just below the NBC and decreases gradually toward the surroundings. This occurrence of boiling in the uppermost subseafloor near the NBC can be confirmed by consistency with the observations that all the vents in the study area, including the NBC, emit white fumes (i.e., white smokers) (Chiba et al., 1996) and that many of the vent fluids in this area were Cl-depleted (Kawagucci et al., 2011).

To further check the validity of the calculation model, a sensitivity analysis was implemented as described in Text S3 (see also Figures S2 and S3). Models without either the conduit or caprock could not reproduce the measured temperatures and heat fluxes. This mismatch was caused by the nonoccurrence of lateral flows in the shallow subseafloor. Additionally, in the absence of the caprock, boiling could not be induced because of the large temperature decrease caused by deep infiltration of seawater. Consequently, the importance of the conduit and caprock for hydrothermal fluid flow and their correct setting in this study were demonstrated.

Distributions of massive and granular sulfide minerals were observed near the NBC seafloor (Site C0016) and near the shallow subseafloor of Sites C0013 and C0014 (Yeats et al., 2017), and the formation of two-layered SMS deposits was estimated by Ishizu et al. (2019), as mentioned above. This two-layered structure can be considered to have been caused by the boiling of hydrothermal fluids and lateral flows in the shallow subseafloor. Both the simulation result and field observations suggested the occurrence of two-phase separation into vapor- and liquid-rich fluids in the uppermost subseafloor near the NBC. Through this phase separation, metal components in the fluids become concentrated in the liquid phase, and sulfide minerals precipitate (Kawagucci et al., 2013) by the fractionation of chemical species, the pH of the fluids increases, and metal solubility decreases (Drummond & Ohmoto, 1985). The vapor-rich, light fluids poor in metal components ascend and are probably discharged from the vents, which is concordant with the fact that all the vents in the study area are white smokers, as mentioned above, in which scarce sulfide minerals are contained. Therefore, sulfide minerals on the seafloor likely precipitated from past black smokers. At the same time, the liquid-rich fluids are trapped below the caprock, as confirmed through a drilling survey (Kawagucci et al., 2013), and their lateral flows must have caused sulfide mineral precipitation. Note that the NaCl concentration in fluid affects the phase relations, density, and miscibility of the fluid (Ingebritsen et al., 2010). Accordingly, a simulation that considers a binary H_2O-NaCl system is desirable for more accurate modeling of fluid flow, as demonstrated by a previous study (Lewis, 2007). This simulation is our significant next step.

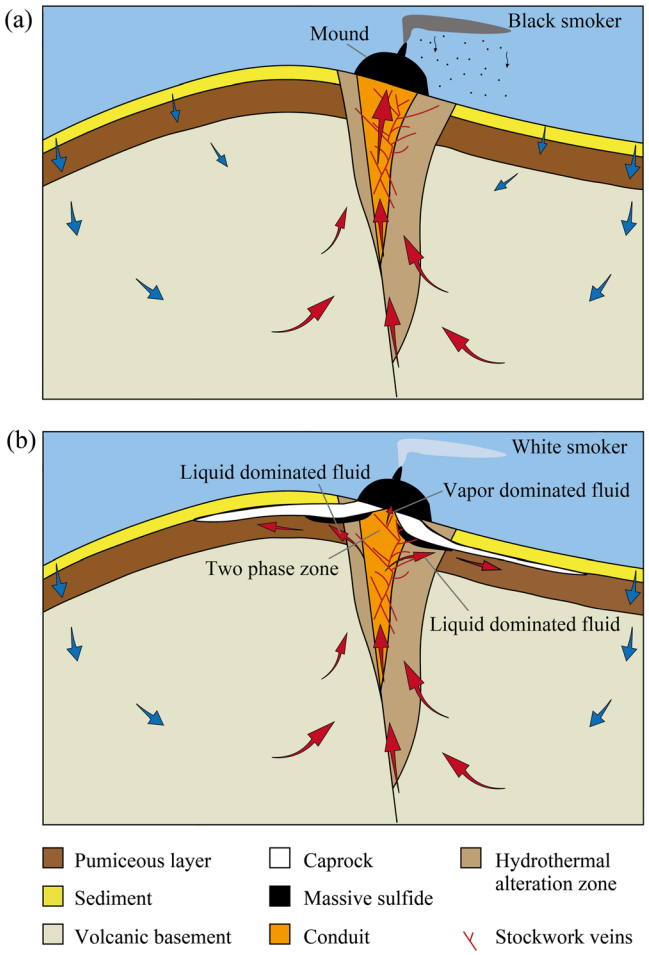

Figure 4. Conceptual model of the two-stage mineralization process. (a) Early-stage mineralization model in which black smokers discharging from the seafloor were cooled by the seawater and sulfide minerals precipitated from the vents, forming SMS deposits on the seafloor. Long-term precipitation formed a mound around the vent. (b) Late-stage mineralization model in which impermeable portions composed of anhydrite and the clay minerals-bearing mound, and sediment induces lateral flows and boiling of fluids in the conduit top. Gas-phase dominated fluids are discharged from the vent as a white smoker. In contrast, liquid-phase dominated fluids rich in metal components flow laterally below the caprock and form the lower ore body because of boiling and/or conductive cooling. The blue and red arrows denote fluid flows of relatively low- and high-temperature seawaters, respectively.

Based on the above considerations, we propose a two-stage generation scenario of the two-layered SMS deposit in the Iheya North Knoll as follows. In the early stage, high-temperature hydrothermal fluids ascended along the conduit and discharged from the vents as black smokers without boiling below the seafloor, and considerable amounts of sulfide minerals then precipitated on the seafloor from the black smokers by mixing with the seawater (Figure 4a). Long-term precipitation formed a mound and that mound acted to seal the hydrothermal fluid flows in the later stage; consequently, the fluid flows became concentrated in the vent (Fouquet, 1997; Tivey, 2007). The sealing was intensified by the distribution of low-permeability hemipelagic sediments in the shallow subseafloor around the mound. Through mixing of the hydrothermal fluids with the seawater in the mound, anhydrite precipitated and filled the rock voids under fluid temperatures of 200°C or more (Fouquet, 1997; Ishibashi et al., 2017). In addition, the rocks were hydrothermally altered and changed partly to clay minerals with decreasing permeability (Takahashi, 1995). These rocks containing anhydrite and clay minerals in voids became impermeable caprock, which blocked mixing of the hydrothermal fluids and seawater; in addition, the conduit top gradually became less permeable, resulting in flow being diverted horizontally (Koski et al., 1994; Tivey et al., 1995) into the highly permeable volcaniclastic layer (Figure 4b). Because of the effect of the caprock to suppress mixing, the fluid temperature increased, and consequently, boiling occurred at the conduit top, and vapor-rich fluids were discharged from the vents as white smokers, as is occurring at present. At the same time, the liquid-rich fluids rich in metal components flowed laterally under the caprock and precipitated sulfide minerals, mainly by boiling and/or by conductive cooling.

In summary, the controlling factors on the formation of the two-layered SMS deposits are outlined as (i) low-permeability sediments, (ii) decrease in permeability in the shallow subseafloor area, (iii) presence of a high-permeability felsic layer that originated from magmatic eruptions, and (iv) shallow water depth. Note that the presence of a high-permeability layer is a common indicator of high magmatic activity in arc volcanos and back-arc basins with eruptions. Regarding the water depth, hydrothermal fields in arc volcanos and back-arc basins are generally situated within a depth of 2,000 m, much shallower than the typical hydrothermal fields in mid-ocean ridges at 2,000 to 3,000 m depths (Hannington et al., 2005). Because the Iheya North Knoll is located at about 1,000 m depth, pore waters at shallow depths are less pressurized. These pressure conditions are favorable to boiling of the fluids, and consequently, the formation of the two-layered structure.

4. Conclusions

In this study, a simple, but essential subseafloor geologic model was constructed to clarify the regional temperature, fluid-flow patterns, and physical property distributions in a hydrothermal system of a back-arc basin, by selecting the Iheya North Knoll, middle Okinawa Trough, southwest Japan, as an example. This clarification was achieved by a numerical simulation of multiphase fluid using TOUGH2 with geological, hydrological, and thermal constraints. The model was well constrained by the survey data of temperature logging and drilling at several points and dense heat fluxes that are rarely obtained in seafloor hydrothermal systems. Therefore, the simulation result can contribute to clarifying subseafloor flow patterns and physical conditions more accurately and interpreting geophysical images such as marine electrical resistivity topography based on the temperature distribution. The most important finding of this study is that the fluid flow is

essentially controlled by the presence of a caprock layer and conduit. The resultant flow features were that the hydrothermal fluids ascend along the conduit toward the seafloor and a portion of them flow laterally below the caprock, as observed by a drilling survey. Because of the presence of the caprock and conduit, the calculated temperatures and heat fluxes were consistent with the measured ones, and the boiling location was in accord with the observed one.

In the study area, development of the two-layered SMS deposit in the study area was interpreted using electrical resistivity tomography. Based on the simulation results and the preceding measurements and observations, a generation mechanism of this two-layered SMS deposit was proposed as formation by two stages of mineralization. In the early stage, hydrothermal fluids were discharged as black smokers rich in metals, and by mixing with the seawater, sulfide minerals from the smokers were deposited on the seafloor. In the later stage, the conduit gradually became less permeable over time, which induced lateral flows in a highly permeable volcaniclastic layer, and consequently, caprock was generated by the precipitation of anhydrite and clay minerals in the layer. Because of the caprock, the temperature of the hydrothermal fluids increased and boiling occurred. The vapor-rich fluids were discharged as white smokers from the vents, whereas the liquid-rich fluids, flowing laterally below the caprock, formed the lower SMS deposits mainly by boiling.

Data Availability Statement

Data is available through Takai et al. (2011) and Masaki et al. (2011).

Acknowledgments
This work was financially supported by the Cross-ministerial Strategic Innovation Promotion Program (SIP). Valuable comments and suggestions by the Associate Editor and an anonymous reviewer are sincerely appreciated.

References

Alt, J. C. (1995). Subseafloor processes in mid-ocean ridge hydrothermal systems. In S. E. Humphris, R. A. Zierenberg, L. S. Mullineaux, R. E. Thomson (Eds.), *Seafloor hydrothermal systems: Physical, chemical, biological, and geological interactions* (Vol. 91, pp. 85–114). Washington, DC: American Geophysical Union. https://doi.org/10.1029/GM091p0085

Arai, R., Kodaira, S., Takahashi, T., Miura, S., & Kaneda, Y. (2018). Seismic evidence for arc segmentation, active magmatic intrusions and syn-rift fault system in the northern Ryukyu volcanic arc. *Earth, Planets and Space*, *70*(1), 61. https://doi.org/10.1186/s40623-018-0830-8

Bardi, U., Jakobi, R., & Hettiarachchi, H. (2016). Mineral resource depletion: A coming age of stockpiling? *BioPhysical Economics and Resource Quality*, *1*(1), 4. https://doi.org/10.1007/s41247-016-0004-x

Chiba, H., Ishibashi, J., Ueno, H., Oomori, T., Uchiyama, N., Takeda, T., et al. (1996). Seafloor hydrothermal systems at North Knoll, Iheya Ridge, Okinawa Trough. *JAMSTEC Journal of Deep Sea Research*, *12*, 211–219.

Coogan, L., Howard, K., Gillis, K., Bickle, M., Chapman, H., Boyce, A., et al. (2006). Chemical and thermal constraints on focussed fluid flow in the lower oceanic crust. *American Journal of Science*, *306*(6), 389–427. https://doi.org/10.2475/06.2006.01

Drummond, S., & Ohmoto, H. (1985). Chemical evolution and mineral deposition in boiling hydrothermal systems. *Economic Geology*, *80*(1), 126–147. https://doi.org/10.2113/gsecongeo.80.1.126

Fouquet, Y. (1997). Where are the large hydrothermal sulphide deposits in the oceans? *Philosophical Transactions of the Royal Society A: Mathematical, Physical and Engineering Sciences*, *355*(1723), 427–441. https://doi.org/10.1098/rsta.1997.0015

Hannington, M., Jamieson, J., Monecke, T., Petersen, S., & Beaulieu, S. (2011). The abundance of seafloor massive sulfide deposits. *Geology*, *39*(12), 1155–1158. https://doi.org/10.1130/G32468.1

Hannington, M. D., de Ronde, C. E. J., & Petersen, S. (2005). Sea-floor tectonics and submarine hydrothermal systems. In J. W. Hedenquist, J. F. H. Thompson, R. J. Goldfarb, J. P. Richards (Eds.), *Economic geology 100th anniversary volume* (pp. 111–141). Littleton, Colorado: Society of Economic Geologists, Inc. http://eprints.uni-kiel.de/id/eprint/6271

Ingebritsen, S. E., Geiger, S., Hurwitz, S., & Driesner, T. (2010). Numerical simulation of magmatic hydrothermal systems. *Reviews of Geophysics*, *48*, RG1002. https://doi.org/10.1029/2009RG000287

Ishibashi, J., Yanagikawa, K., & Takai, K. (2017). A new model for a hydrothermal circulation system and limit of the life (in Japanese with English abstract). *The Journal of the Geological Society of Japan*, *123*(4), 237–250. https://doi.org/10.5575/geosoc.2017.0014

Ishizu, K., Goto, T., Ohta, Y., Kasaya, T., Iwamoto, H., Vachiratienchai, C., et al. (2019). Internal structure of a seafloor massive sulfide deposit by electrical resistivity tomography, Okinawa Trough. *Geophysical Research Letters*, *46*, 11,025–11,034. https://doi.org/10.1029/2019GL083749

Kawagucci, S., Chiba, H., Ishibashi, J., Yamanaka, T., Toki, T., Muramatsu, Y., et al. (2011). Hydrothermal fluid geochemistry at the Iheya North field in the mid-Okinawa Trough: Implication for origin of methane in subseafloor fluid circulation systems. *Geochemical Journal*, *45*(2), 109–124. https://doi.org/10.2343/geochemj.1.0105

Kawagucci, S., Miyazaki, J., Nakajima, R., Nozaki, T., Takaya, Y., Kato, Y., et al. (2013). Post-drilling changes in fluid discharge pattern, mineral deposition, and fluid chemistry in the Iheya North hydrothermal field, Okinawa Trough. *Geochemistry, Geophysics, Geosystems*, *14*, 4774–4790. https://doi.org/10.1002/2013GC004895

Koski, R. A., Jonasson, I. R., Kadko, D. C., Smith, V. K., & Wong, F. L. (1994). Compositions, growth mechanisms, and temporal relations of hydrothermal sulfide-sulfate-silica chimneys at the northern Cleft segment, Juan de Fuca Ridge. *Journal of Geophysical Research*, *99*(B3), 4813–4832. https://doi.org/10.1029/93JB02871

Lewis, K. C. (2007). Numerical modeling of two-phase flow in the sodium chloride-water system with applications to seafloor hydrothermal systems, (doctoral dissertation). Retrieved from SMARTech repository. (https://smartech.gatech.edu/handle/1853/19810). Atlanta: Georgia Institute of Technology.

Lipton, I. (2012). Mineral Resource Estimate Solwara Project, Bismarck Sea PNG (Technical Report NI43-101). Retrieved from http://www.nautilusminerals.com/irm/content/pdf/SL01-NSG-DEV-RPT-7020-001_Rev_1_Golder_Resource_Report.pdf

Lowell, R. P., & Yao, Y. (2002). Anhydrite precipitation and the extent of hydrothermal recharge zones at ocean ridge crests. *Journal of Geophysical Research*, *107*(B9), 2183. https://doi.org/10.1029/2001JB001289

Lowell, R. P., Yao, Y., & Germanovich, L. N. (2003). Anhydrite precipitation and the relationship between focused and diffuse flow in seafloor hydrothermal systems. *Journal of Geophysical Research*, *108*(B9), 2404. https://doi.org/10.1029/2002JB002371

Lusty, P., & Gunn, A. (2015). Challenges to global mineral resource security and options for future supply. *Geological Society, London, Special Publications*, *393*(1), 265–276. https://doi.org/10.1144/SP393.13

Masaki, Y., Kinoshita, M., Inagaki, F., Nakagawa, S., & Takai, K. (2011). Possible kilometer-scale hydrothermal circulation within the Iheya-North field, mid-Okinawa Trough, as inferred from heat flow data. *JAMSTEC Report of Research and Development*, *12*, 1–12. https://doi.org/10.5918/jamstecr.12.1

Pruess, K., Oldenburg, C. M., & Moridis, G. (1999). TOUGH2 user's guide version 2 (Rep. LBNL-43134). Berkeley, CA: Lawrence Berkeley National Laboratory. https://doi.org/10.2172/751729

Sahlström, F., Dirks, P., Chang, Z., Arribas, A., Corral, I., Obiri-Yeboah, M., & Hall, C. (2018). The Paleozoic Mount Carlton Deposit, Bowen Basin, Northeast Australia: Shallow high-sulfidation epithermal Au-Ag-Cu mineralization formed during rifting. *Economic Geology*, *113*(8), 1733–1767. https://doi.org/10.5382/econgeo.2018.4611

Saito, S., Sanada, Y., Moe, K., Kido, Y. N., Hamada, Y., Kumagai, H., et al. (2015). Identification and characterization of the active hydrothermal deposits in Okinawa Trough, SW Japan: Estimates from logging-while-drilling. AGU Fall Meeting Abstracts. San Francisco. Retrieved from. https://agu.confex.com/agu/fm15/webprogram/Paper77585.html

Spagnoli, G., Hannington, M., Bairlein, K., Hördt, A., Jegen, M., Petersen, S., & Laurila, T. (2016). Electrical properties of seafloor massive sulfides. *Geo-Marine Letters*, *36*(3), 235–245. https://doi.org/10.1007/s00367-016-0439-5

Stein, C. A., & Stein, S. (1992). A model for the global variation in oceanic depth and heat flow with lithospheric age. *Nature*, *359*(6391), 123–129. https://doi.org/10.1038/359123a0

Takahashi, H. (1995). Alteration cap rock formation model—A case study Hosokura ore deposits in northeastern Japan—(in Japanese with English abstract). *Journal of the Geothermal Research Society of Japan*, *17*(4), 271–284. https://doi.org/10.11367/grsj1979.17.271

Takai, K., Mottl, M., Nielsen, S., & the Expedition 331 Scientists (2010). *Deep hot biosphere*. (*Integrated Ocean Drilling Program Preliminary Report, 331*). Tokyo: Integrated Ocean Drilling Program Management International, Inc. https://doi.org/10.2204/iodp.pr.331.2010

Takai, K., Mottl, M., Nielsen, S., & the Expedition 331 Scientists (2011). *Proceedings of the integrated ocean drilling program* (Vol. 331). Tokyo: Integrated Ocean Drilling Program Management International, Inc. https://doi.org/10.2204/iodp.proc.331.2011

Takai, K., & Nakamura, K. (2010). Compositional, physiological and metabolic variability in microbial communities associated with geochemically diverse, deep-sea hydrothermal vent fluids. In L. L. Barton, M. Mandl, A. Loy (Eds.), *Geomicrobiology: Molecular and environmental perspective* (pp. 251–283). Dordrecht: Springer. https://doi.org/10.1007/978-90-481-9204-5_12

Tivey, M. A., & Johnson, H. P. (2002). Crustal magnetization reveals subsurface structure of Juan de Fuca Ridge hydrothermal vent fields. *Geology*, *30*(11), 979–982. https://doi.org/10.1130/0091-7613(2002)030<0979:CMRSSO>2.0.CO;2

Tivey, M. K. (2007). Generation of seafloor hydrothermal vent fluids and associated mineral deposits. *Oceanography*, *20*(1), 50–65. https://doi.org/10.5670/oceanog.2007.80

Tivey, M. K., Humphris, S. E., Thompson, G., Hannington, M. D., & Rona, P. A. (1995). Deducing patterns of fluid flow and mixing within the TAG active hydrothermal mound using mineralogical and geochemical data. *Journal of Geophysical Research*, *100*(B7), 12,527–12,555. https://doi.org/10.1029/95JB00610

Tornos, F., Peter, J. M., Allen, R., & Conde, C. (2015). Controls on the siting and style of volcanogenic massive sulphide deposits. *Ore Geology Reviews*, *68*, 142–163. https://doi.org/10.1016/j.oregeorev.2015.01.003

Tsuji, T., Takai, K., Oiwane, H., Nakamura, Y., Masaki, Y., Kumagai, H., et al. (2012). Hydrothermal fluid flow system around the Iheya North Knoll in the mid-Okinawa trough based on seismic reflection data. *Journal of Volcanology and Geothermal Research*, *213-214*, 41–50. https://doi.org/10.1016/j.jvolgeores.2011.11.007

Yeats, C. J., Hollis, S. P., Halfpenny, A., Corona, J., LaFlamme, C., Southam, G., et al. (2017). Actively forming Kuroko-type volcanic-hosted massive sulfide (VHMS) mineralization at Iheya North, Okinawa Trough, Japan. *Ore Geology Reviews*, *84*, 20–41. https://doi.org/10.1016/j.oregeorev.2016.12.014

Yoshizumi, R., Miyoshi, Y., & Ishibashi, J. (2015). The characteristics of the seafloor massive sulfide deposits at the Hakurei Site in the Izena Hole, the Middle Okinawa Trough. In J. Ishibashi, K. Okino, M. Sunamura (Eds.), *Subseafloor biosphere linked to hydrothermal systems* (pp. 561–565). Tokyo: Springer. https://doi.org/10.1007/978-4-431-54865-2_43

References From the Supporting Information

Bear, J. (1972). *Dynamics of fluids in porous media*. New York: American Elsevier.

Converse, D., Holland, H., & Edmond, J. (1984). Flow rates in the axial hot springs of the East Pacific Rise (21 N): Implications for the heat budget and the formation of massive sulfide deposits. *Earth and Planetary Science Letters*, *69*(1), 159–175. https://doi.org/10.1016/0012-821X(84)90080-3

Coumou, D., Driesner, T., & Heinrich, C. A. (2008). The structure and dynamics of mid-ocean ridge hydrothermal systems. *Science*, *321*(5897), 1825–1828. https://doi.org/10.1126/science.1159582

Elderfield, H., & Schultz, A. (1996). Mid-ocean ridge hydrothermal fluxes and the chemical composition of the ocean. *Annual Review of Earth and Planetary Sciences*, *24*(1), 191–224. https://doi.org/10.1146/annurev.earth.24.1.191

Fehn, U., & Cathles, L. M. (1979). Hydrothermal convection at slow-spreading mid-ocean ridges. *Tectonophysics*, *55*(1–2), 239–260. https://doi.org/10.1016/0040-1951(79)90343-3

Fisher, A., Becker, K., & Narasimhan, T. (1994). Off-axis hydrothermal circulation: Parametric tests of a refined model of processes at Deep Sea Drilling Project/Ocean Drilling Program site 504. *Journal of Geophysical Research*, *99*(B2), 3097–3121. https://doi.org/10.1029/93JB02741

Freeze, R. A., & Cherry, J. A. (1979). *Groundwater*. Englewood Cliffs, NJ: Prentice Hall.

Gruen, G., Weis, P., Driesner, T., Heinrich, C. A., & de Ronde, C. E. J. (2014). Hydrodynamic modeling of magmatic–hydrothermal activity at submarine arc volcanoes, with implications for ore formation. *Earth and Planetary Science Letters*, *404*, 307–318. https://doi.org/10.1016/j.epsl.2014.07.041

LaFlamme, B., Delaney, J. R., McDuff, R. E., Miller, V., Robigou, V., Schultz, A., et al. (1989). Observations and experimental studies in the Endeavour hydrothermal field-summer 1988. *Eos, Transactions of the American Geophysical Union*, *70*, 1160–1161.

Magri, F., Akar, T., Gemici, U., & Pekdeger, A. (2010). Deep geothermal groundwater flow in the Seferihisar–Balçova area, Turkey: Results from transient numerical simulations of coupled fluid flow and heat transport processes. *Geofluids*, *10*(3), 388–405. https://doi.org/10.1111/j.1468-8123.2009.00267.x

Raharjo, I. B., Allis, R. G., & Chapman, D. S. (2016). Volcano-hosted vapor-dominated geothermal systems in permeability space. *Geothermics*, *62*, 22–32. https://doi.org/10.1016/j.geothermics.2016.02.005

Rona, P. A., & Trivett, D. A. (1992). Discrete and diffuse heat transfer at ASHES vent field, Axial Volcano, Juan de Fuca Ridge. *Earth and Planetary Science Letters*, *109*(1–2), 57–71. https://doi.org/10.1016/0012-821X(92)90074-6

Schultz, A., Delaney, J., & McDuff, R. (1992). On the partitioning of heat flux between diffuse and point source seafloor venting. *Journal of Geophysical Research*, *97*(B9), 12,299–12,314. https://doi.org/10.1029/92JB00889

Schultz, A., & Elderfield, H. (1999). Controls on the physics and chemistry of seafloor hydrothermal circulation. In J. R. Cann, H. Elderfield, A. Laughton (Eds.), *Mid-ocean ridges, dynamics of processes associated with creation of new oceanic crust* (pp. 171–210). Cambridge, UK: Cambridge University Press. https://doi.org/10.1017/CBO9780511600050.009

Yang, J., Edwards, R., Molson, J. W., & Sudicky, E. (1996). Three-dimensional numerical simulation of the hydrothermal system within TAG-like sulfide mounds. *Geophysical Research Letters*, *23*(23), 3475–3478. https://doi.org/10.1029/96GL03081